Multi-material 3D printing of functionally graded soft-hard interfaces for enhancing mandibular kinematics of temporomandibular joint replacement prostheses

Moosabeiki, Vahid; Khan, Afaq; Cruz Saldivar, Mauricio; Van Paepegem, Wim; Jonker, Brend P.; Wolvius, Eppo B.; Zhou, Jie; Tumer, Nazli; Mirzaali, Mohammad J.; Zadpoor, Amir A.

DOI
10.1038/s43246-024-00664-4

Publication date
2024

Document Version
Final published version

Published in
Communications Materials

communications materials

Article

https://doi.org/10.1038/s43246-024-00664-4

Multi-material 3D printing of functionally graded soft-hard interfaces for enhancing mandibular kinematics of temporomandibular joint replacement prostheses

Vahid Moosabeiki[1] ✉, Afaq Khan[1], Mauricio Cruz Saldivar[1], Wim Van Paepegem[2], Brend P. Jonker[3], Eppo B. Wolvius[3], Jie Zhou[1], Nazli Tumer[1], Mohammad J. Mirzaali[1] ✉ & Amir A. Zadpoor[1]

Temporomandibular joint (TMJ) replacement prostheses often face limitations in accommodating translational movements, leading to unnatural kinematics and loading conditions, which affect functionality and longevity. Here, we investigate the potential of functionally graded materials (FGMs) in TMJ prostheses to enhance mandibular kinematics and reduce joint reaction forces. We develop a functionally graded artificial cartilage for the TMJ implant and evaluate five FGM designs: hard, hard-soft, and three FGM gradients with gradual transitions from 90% hard material to 0%, 10%, and 20%. These designs are 3D printed, mechanically tested under quasi-static compression, and simulated under physiological conditions. Results from computational modeling and experiments are compared to an intact mandible during incisal clenching and left group biting. The FGM design with a transition from 90% to 0% hard material improves kinematics by 19% and decreases perfomance by 3%, reduces joint reaction forces by 8% and 10%, and increases mandibular movement by 20% and 88% during incisal clenching and left group biting, respectively. These findings provide valuable insights for next-generation TMJ implants.

The temporomandibular joint (TMJ) is an important part of the human masticatory system. It supports such functions as chewing, speaking, swallowing, and facial expressions[1,2]. Anatomically, the TMJ is a complex structure including the mandibular condyle, articular disc, and temporal bone socket, all working together to facilitate smooth and coordinated movements[3]. The TMJ allows for rotational movement in the sagittal plane and translational movement along its own axis. Proper functioning of the TMJ is necessary for maintaining overall oral health and well-being[4,5]. However, disorders and injuries can impact the TMJ, leading to significant pain and dysfunction[5,6] and, thus, might require surgical interventions with the use of TMJ prostheses.

Current TMJ total joint replacement (TJR) prostheses have several clinical limitations[7]. These prostheses typically allow primarily rotational movements but have limitations in accommodating translational movements, which leads to unnatural kinematics and inefficient loading conditions for the prosthetic joint[8–15]. Furthermore, while these prostheses offer an adequate movement range for daily activities, they do not achieve the mobility levels seen in healthy individuals[16,17]. This gap highlights the necessity for developing advanced TMJ prostheses that can more accurately replicate the natural joint mechanics and improve the functional outcomes for patients. Moreover, many current TMJ prosthesis designs include a metallic structure (i.e., the mandibular component which is typically made of a titanium alloy for the shaft and a cobalt-chromium-molybdenum alloy for the articulating surface) and a polymeric fossa component (*e.g.*, ultra-high molecular weight polyethylene (UHMWPE)), which can lead to issues, such as wear, slippage, and degradation over time, thereby affecting the

[1]Department of Biomechanical Engineering, Faculty of Mechanical Engineering, Delft University of Technology (TU Delft), Mekelweg 2, 2628 CD Delft, The Netherlands. [2]Department of Materials, Textiles and Chemical Engineering, Mechanics of Materials and Structures (MMS), Ghent University, 5092 Ghent, Belgium. [3]Department of Oral and Maxillofacial Surgery, Erasmus University Medical Center, Doctor Molewaterplein 40, 3015 GE Rotterdam, The Netherlands. ✉e-mail: v.moosabeiki@tudelft.nl; m.j.mirzaali@tudelft.nl

longevity and functionality of such prostheses[8,10,13,18,19]. The functional outcomes of TMJ arthroplasty are evaluated mainly in terms of restoring function, maintaining prosthesis fixation, and minimizing the degradation of the prosthetic components and surrounding bone and soft tissue[11]. It is expected that addressing the limitations of the current TMJ prostheses will considerably improve their functional outcomes.

Functionally graded materials (FGMs) have emerged as a generation of engineered materials to serve the specific needs of many structural parts and may offer a promising solution to address the limitations of the current TMJ prostheses[20,21]. These materials are found in biological structures, such as bone, teeth, and interface tissues, such as cartilage-to-bone interfaces at the end of the condyle in the mandible[21–28]. FGMs are characterized by a gradual variation in composition and/or structure over their volume, which allows for the tailoring of their properties to meet specific functional requirements[29]. This gradation can be achieved through various means, including porosity gradients, compositional or chemical, and/or microstructural gradients[30]. One of the key advantages of FGMs over traditional composites, such as layered composites, is their ability to eliminate abrupt hard-soft interfaces[23,24]. Discrete interfaces in layered composites often lead to stress concentrations, which can compromise the structural integrity and longevity of the composites[31–33]. FGMs, on the other hand, provide a smoother transition between different material properties, thereby mitigating the stress concentrations and enhancing the overall performance of such materials, especially under repetitive loading conditions. While the concept of FGMs for implants is well known, including dental[34] and other joint implants (e.g., knee and ankle prostheses[35,36] and hip stem implants[37,38]), their clinical implementation has been limited due to the obstacles related to the fabrication costs and difficulties of applying FGMs to complexly shaped implants. The feasibility of applying FGMs to TMJ replacement prostheses for alloplastic reconstruction of the mandible is yet to be explored[39].

Here, we propose a methodology to incorporate FGM design concepts into TMJ prostheses. We hypothesized that such an implementation enhances the mandibular kinematics and reduces joint reaction forces. Toward this purpose, we designed, additively manufactured, and mechanically tested various FGM configurations with different material property distributions, and identified designs that better replicate the natural movements of the TMJ while maintaining the distribution of the stresses more evenly across the joint. We also employed experimentally validated finite element models to evaluate the performance of those TMJ prosthesis designs under relevant physiological conditions corresponding to the incisal clenching (INC) and left group biting (LGF). Finally, using finite element analysis (FEA) we investigated the stress and strain distributions and potential points of failure when incorporating such FGM concepts in the design of TMJ prostheses.

The significance of this study lies in its potential to contribute to the development of more tissue-mimetic TMJ implants for future clinical applications. By addressing the current limitations and exploring these design strategies, we aim to improve the functional outcomes for the patients requiring TMJ replacement through the design and implementation of FGM-incorporated prostheses for TMJ reconstruction.

Results and discussion

In this study, we explored how FGMs could enhance the biomechanical performance of TMJ prostheses, focusing on the kinematics and reaction forces of prostheses. We developed and implemented various designs of artificial cartilage attached to the proximal part of the TMJ implants (Fig. 1a). The modifications in those designs aimed to enhance the contact interface between the TMJ implant and the fossa component, based on the structurally optimized TMJ implant designs introduced in a previous study[40]. The initial TMJ implant design had a gap between the implant head and the liner, which could cause some rigid body movements of the implant (Fig. 1b)[12]. To resolve this issue, we added ten layers of materials with different elastic moduli to act as artificial cartilage and ensure a close-fitting contact between the articulating surfaces, thereby limiting any rigid body movement of the TMJ implant head (Fig. 1b, c). Consequently, the liner was also modified to fit the layers and avoid any gaps or clearances between the TMJ implant head and the liner (Fig. 1b).

The computational model was validated by using three methods. First, we compared the maximum principal logarithmic strain in the linear elastic range (corresponding to a bar displacement of 1.5 mm), as predicted by the FEA model with the maximum principal true strain measured using DIC (Fig. 2a, c). Second, we compared the force-displacement graphs (Fig. 2b). Lastly, we compared the x and y displacements of the sixth screw (Fig. 2a) relative to the bar displacement (i.e., the z-displacement) between FEA and DIC (Fig. 2d).

High strains were observed on the implants together with the cartilage-mimicking component around the condylar neck and near the resection border on the superior side of the first and second screws (Fig. 2a). The strain contour plots from DIC and FEA on the ramus area showed similar distributions, with strain values in the three regions (i.e., sigmoid notch, posterior border of the ramus, and mandibular angle) closely matching by factors of 1.07 and 1.3 for the intact mandible and the implant with a hard-soft cartilage-mimicking component, respectively (Fig. 2c). Pearson's correlation coefficients of $r = 0.99$ for the intact mandible and $r = 0.94$ for the implant with the hard-soft cartilage indicated a strong linear correlation between DIC measurements and FEA predictions (Fig. 2c).

Prothesis performance

When comparing the strain distribution among the three designs of the cartilage-mimicking component (*i.e.*, hard, hard-soft, and FGM[90–0]), the FGM designs demonstrated the evenest strain distribution in the mandibular angle (Fig. 2a) and the cartilage-mimicking component (Fig. 2e). In the hard-soft design, which featured an abrupt transition between the hard and soft materials, stress concentrations were detected at the interface of both materials, as evidenced by a more than ninefold increase of the stress value (from 0.37 to 3.42 MPa) (Fig. 2e). This stress concentration could initiate cracks and delamination at the interfaces, thereby affecting the long-term performance and durability of the prosthesis[30,33].

The force-displacement results obtained from the quasi-static biomechanical testing and FEA are shown in Fig. 2b. The stiffness values of the implanted mandibles were similar between computational results and experimental measurements, and all were consistently lower than the value of the intact mandible. Specifically, the stiffness of the FGM-implanted mandible was 14% lower than the intact mandible in the FEA and 31% lower in the experimental setup. The forces predicted by the FEA were 1.9 times higher than those measured in the experiment (Fig. 2b). These differences could be attributed to the variations in material properties, as the mechanical properties used in the FEA may not perfectly match those of the actual materials used in the experimental setup. Additionally, variations in experimental measurements and the 3D printing process could contribute to these differences[41].

While this study primarily focused on INC and LGF biting tasks, where bending is more dominant, we acknowledge that twisting (torsional) movements of the mandible may also play an important role in mandibular biomechanics. Twisting can occur during more complex or asymmetric chewing patterns and may introduce additional stress distributions that could further impact the performance of TMJ prostheses. Although our study focused on designing an artificial cartilage and did not explicitly consider twisting movements, future research should incorporate both bending and twisting to provide a more comprehensive understanding of the mechanical behavior of TMJ prostheses under various functional conditions.

Additionally, we acknowledge that while this study reports peak stress values, the effects of bone remodeling were not considered. Bone remodeling can influence stress distribution and implant stability over time, and screw loosening may result from regional bone resorption around the screws, which was not evaluated[42]. Future research should incorporate bone remodeling to better assess long-term stress distribution and screw stability.

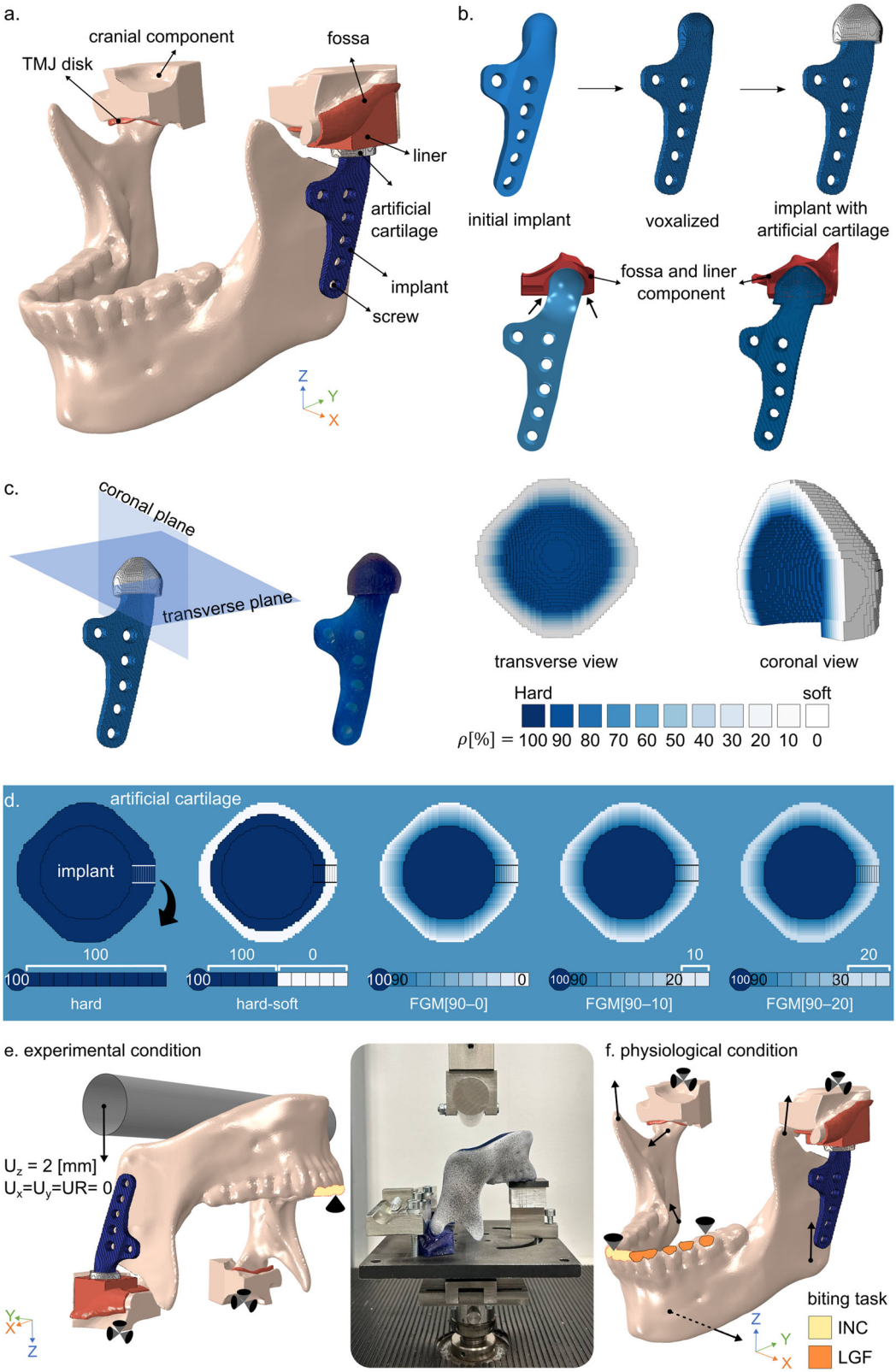

Fig. 1 | Design and material composition of TMJ Implants. a The implanted mandible with artificial cartilage. **b** Initial and modified designs of the TMJ implants and artificial cartilage. **c** The voxelized-FEA model with 10 additional layers of materials acting as artificial cartilage to ensure close-fitting contact between the articulating surfaces and prevent rigid body movements. **d** Various material property distributions within the artificial cartilage, including hard, hard-soft, and multiple FGM designs (e.g., $\rho = 90\%$ to $\rho = 0\%$) (transverse cut view). **e** Experimental configuration (EXP-FEA) and (f) muscle force vectors and constraints used in physiological FEA (PHY-FEA).

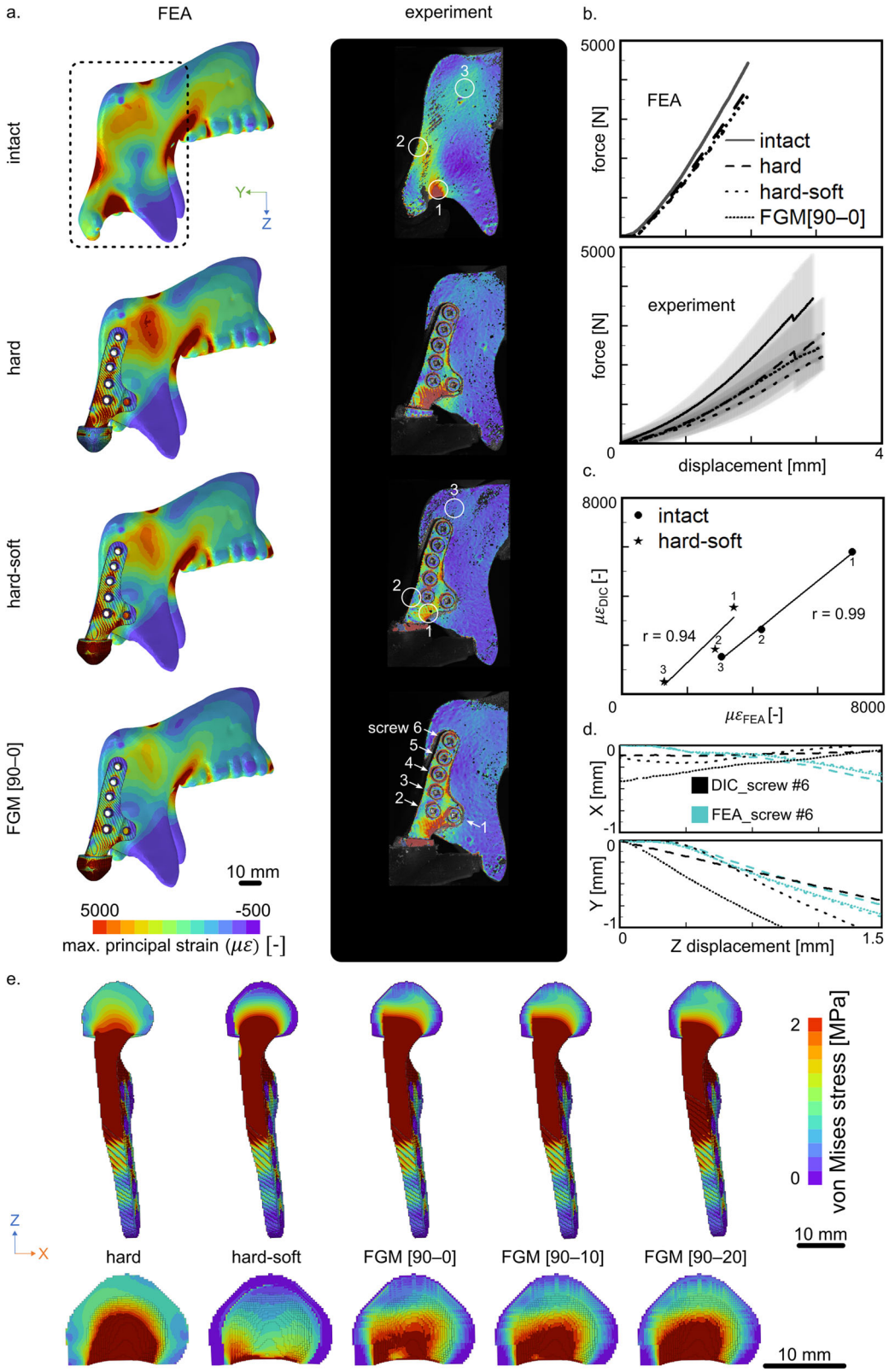

Fig. 2 | Strain/stress distributions and biomechanical testing. a Comparisons between digital image correlation (DIC) and FEA in the strain distributions on the surface of the implant (together with the artificial cartilage), around the condylar neck, and resection border. **b** The results obtained from the quasi-static compression testing for biomechanical evaluation. **c** The Pearson similarity between FEA and DIC in three different regions chosen in (**a**). **d** Comparisons in the *x* and *y* displacements of screw No. 6 with respect to the bar displacement (in the *z*-direction) between FEA and DIC. **e** Von Mises stress distributions of different cartilage designs. The legends in (**b**) apply to (**d**) as well.

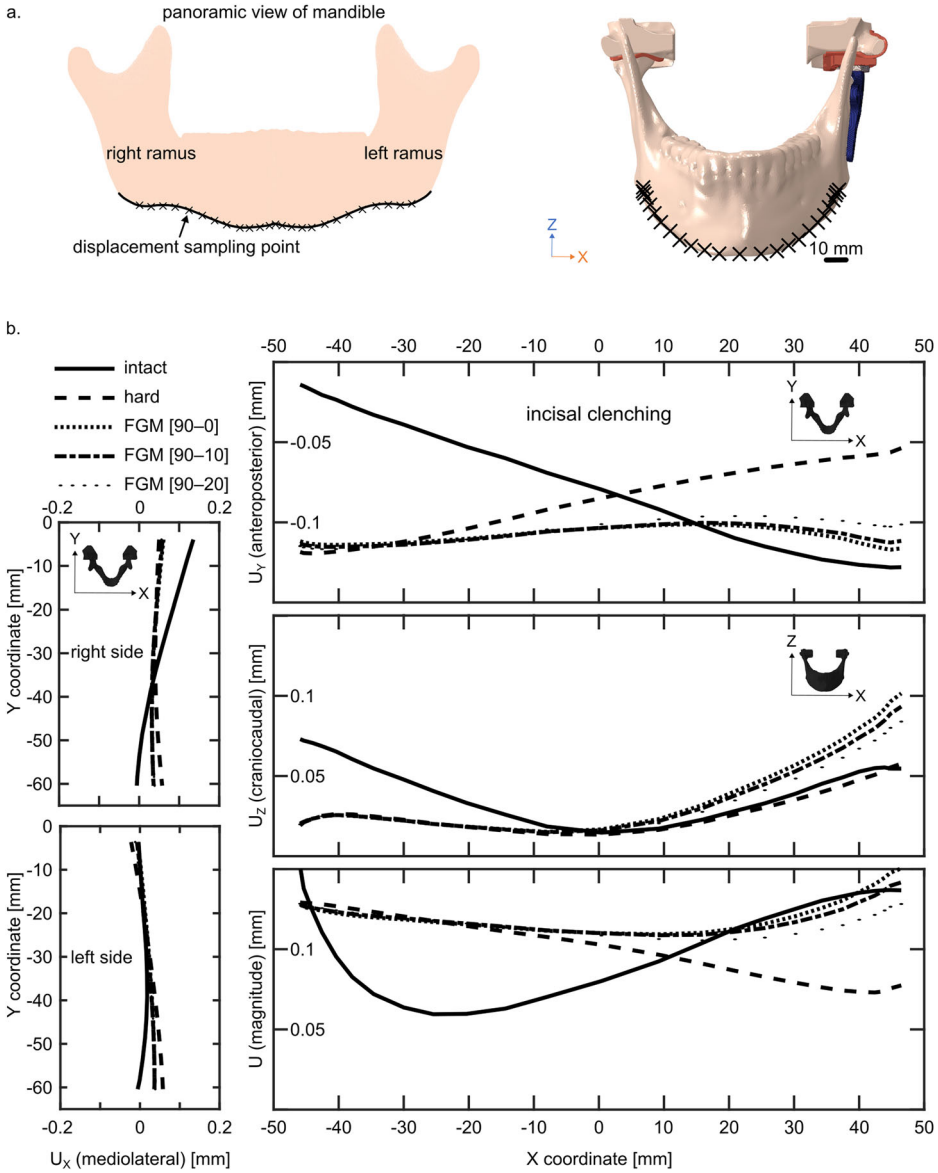

Fig. 3 | Mandibular kinematics during incisal clenching. a The sampling points along the mandible. **b** The mediolateral (U_X), anteroposterior (U_Y), craniocaudal (U_Z), and magnitude displacements of the mandible during incisal clenching for different cartilage designs (hard, FGM[90–0], FGM [90–10], FGM [90–20]).

Kinematics analysis

We assessed the kinematics of four designs of cartilage-mimicking components, *i.e.*, hard, FGM[90–0], FGM [90–10], and FGM [90–20], during the INC task using PHY-FEA, and compared the kinematics of the implanted mandible to that of the intact mandible (Fig. 3). The FGM [90–10] and FGM [90–20] designs were specifically used to evaluate the effect of harder materials. Subsequently, we examined the implanted mandible with hard and FGM[90–0] cartilage-mimicking components and compared them with the intact mandible during the LGF task (Fig. 4).

During the INC, due to the morphological asymmetry of the mandible, the intact mandible tended to move toward the left side. The PHY-FEA showed around a 0.15 mm larger mediolateral (U_X) displacement of the right ramus as compared to the left side (Fig. 3b, left). Moreover, the left side of the mandible moved more anteriorly (U_Y) than the right side during incisal biting, with a displacement of around 0.1 mm (Fig. 3b, right).

Achieving symmetric movement of the mandible is crucial to ensure an even distribution of forces throughout the mandibular structure and its joint[14]. The FGM-incorporated protheses reduced the asymmetry in mediolateral (U_X) movement on the right side and showed a leftward movement in the vicinity of the mandible mental tubercles. They also showed relatively better similarity and closeness to the intact mandible on the left (implanted) side (Fig. 3b-left). In particular, the FGM[90–0] prosthesis achieved a recovery rate of approximately 72% ($\alpha = 0.72$) in the intact mandibular displacement patterns, while the hard cartilage-mimicking components resulted in a recovery rate of only 28% ($\alpha = 0.28$) (Fig. 4b). Furthermore, the mandibular displacement of the FGM[90–0] prosthesis was 4% closer to that of the intact mandible, compared to the prosthesis with a hard cartilage-mimicking component, as indicated by the Euclidean distance values of 0.16 mm for the FGM[90–0] prosthesis and 0.20 mm for the prosthesis with a hard cartilage-mimicking component (Fig. 4b).

During the INC, the anteroposterior (U_Y) movement of the mandibles showed that the hard cartilage-mimicking components resulted in greater anterior movement on the right side (0.12 mm) as compared to the left side (0.05 mm). In contrast, the FGM-incorporated protheses facilitated anterior movement on the left side, resulting in more symmetrical anteroposterior movements of the mandible. Both the left (implanted) and right (intact) sides demonstrated nearly equal anterior movements (0.12 mm) (Fig. 3b, right).

As compared to the prosthesis with the hard cartilage, the FGM-incorporated prostheses, particularly FGM[90–0], reduced the asymmetry in anteroposterior (U_Y) movement (Fig. 3b-right) and demonstrated 28% less dissimilarity ($\alpha = 0.28$) and 7% closer alignment with the displacement

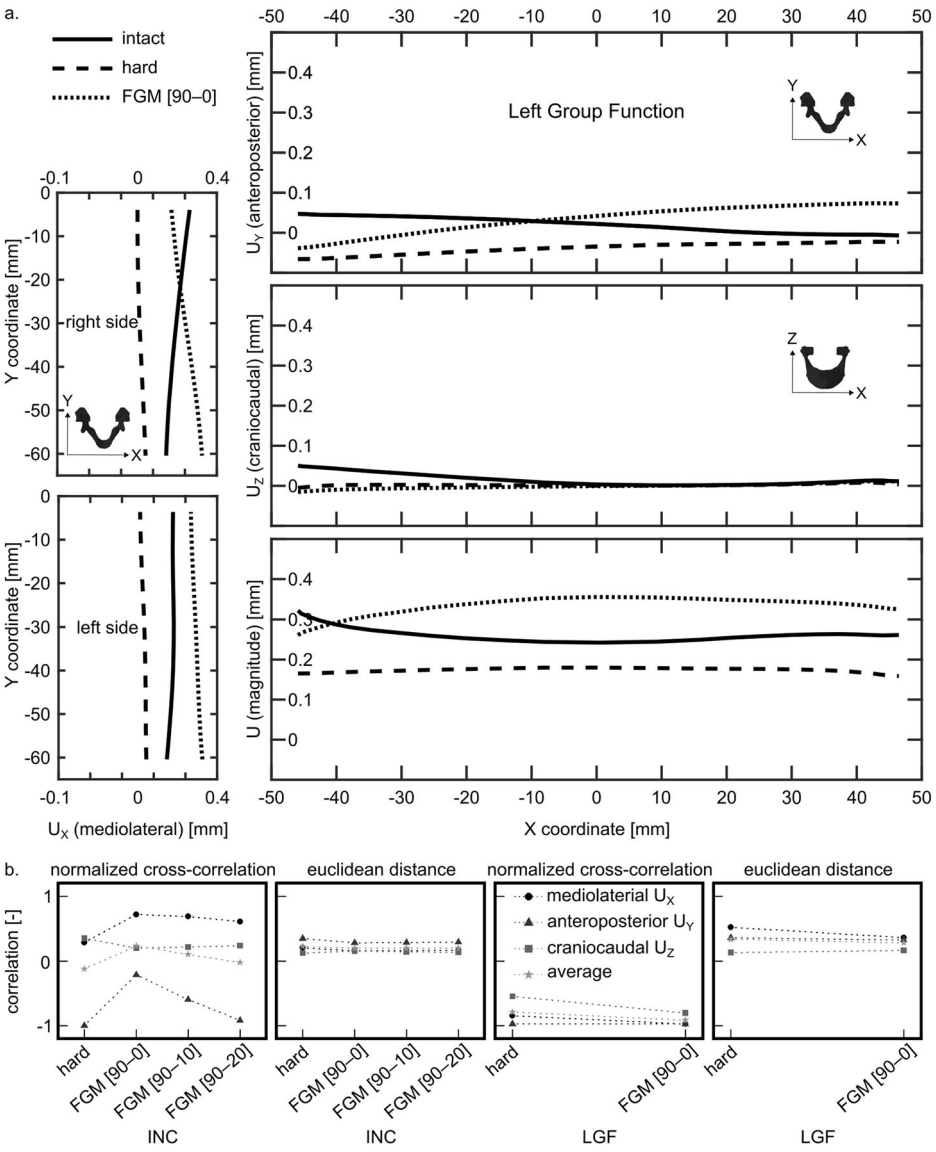

Fig. 4 | Mandibular kinematics during left group biting. a The displacement patterns of hard and FGM[90–0] prostheses (mediolateral, anteroposterior, craniocaudal, and magnitude) during left group biting. **b** The correlation and Euclidean distance between the displacement patterns of the hard, FGM[90–0], FGM [90–10], and FGM [90–20] designs against the intact mandible during the INC and LGF biting tasks.

patterns of the intact mandible (Fig. 4b). The normalized cross-correlation increased from −1 to −0.28 while the Euclidean distance decreased from 0.35 mm to 0.28 mm when comparing the displacements of the intact mandible with those of the prostheses incorporating a hard and an FGM[90–0] cartilage-mimicking component, respectively (Fig. 4b).

The TMJ prosthesis with a hard cartilage-mimicking component showed superior craniocaudal (U_Z) displacement performance during the INC as compared to those with FGM cartilage-mimicking components. The FGM designs of the prostheses, particularly FGM[90–0], resulted in a larger craniocaudal (U_Z) displacement (0.09 mm) on the left side as compared to the design with a hard cartilage-mimicking component (0.05 mm), thus increasing the asymmetry in this specific mandibular movement (Fig. 3b, right). The prosthesis with a hard cartilage-mimicking component resulted in a higher degree of symmetry in the motion of the implanted mandible and enhanced its similarity to the movement pattern observed in the intact mandible. Specifically, the TMJ prosthesis with a hard cartilage-mimicking component recovered 15% more of the intact mandibular displacement patterns than the FGM[90–0] prosthesis (Fig. 4b). Moreover, the prosthesis with a hard cartilage-mimicking component brought this specific movement 3% closer to that of the intact mandible, as indicated by the corresponding Euclidean distances in Fig. 4b.

Among the four designs of the cartilage-mimicking component (Fig. 4b), the FGM[90–0] demonstrated, on average, 36% less dissimilarity and 2% closer alignment to the displacement patterns of the intact mandible as compared to the ones with a hard cartilage-mimicking component. In general, the mandibular movement range during the INC increased when FGM-incorporated prostheses were used, as is clear from the corresponding displacement magnitudes (Fig. 3b, right). The FGM design[90–0] increased the mandibular movement range by 20% (0.02 mm) as compared to the prosthesis with a hard cartilage-mimicking component. The results presented in Fig. 4b also indicate that mandibular displacements could be regulated through a rational distribution of material properties and that the displacement magnitudes increase when the outer layer of the cartilage-mimicking component is relatively softer. Additionally, the reaction forces on the prosthetic joint decreased from 167 N for the hard design of the cartilage-mimicking component to 153 N for the FGM[90–0] design, corresponding to a reduction of >8%.

We further examined the performance of the hard and FGM[90–0] designs of the cartilage-mimicking components during the LGF biting task. Given that mandibular movement during LGF is inherently asymmetric, the concept of symmetry is not applicable here. The intact mandible demonstrated mediolateral (U_X) displacement towards the left side on both the right and left sides (Fig. 4a, left). The right side experienced a greater

craniocaudal (U_Z) displacement of 0.05 mm as compared to the left side, which exhibited a displacement of 0.01 mm (Fig. 4a, right). Additionally, the right side moved posteriorly (U_Y) by 0.05 mm, while the left side showed a slight anterior displacement of 0.01 mm (Fig. 4a, right).

Regarding mediolateral (U_X) displacement during LGF, the hard design of the cartilage-mimicking component decreased the tendency of the implanted mandible to move toward the left (U_X), while the FGM[90–0] design increased it (Fig. 4a, left). As compared with the FGM[90–0] design, the hard design of the cartilage-mimicking component showed a 13% reduction in dissimilarity from the displacement patterns observed in the intact mandible, as indicated by the normalized cross-correlation in Fig. 4b. Conversely, the displacements of the FGM[90–0] design demonstrated a 16% greater degree of proximity to the displacement pattern of the intact mandible, as compared to the hard cartilage design, as shown by the Euclidean distance presented in Fig. 4b.

There is an inversely proportional relationship between the anteroposterior (U_Y) displacements exhibited by the implanted mandibles and those of the intact mandible during LGF. The hard and FGM[90-0] designs showed nearly equal dissimilarity to the displacement field of the intact mandible, with a correlation coefficient (α) of approximately −0.97. However, the FGM[90–0] design demonstrated 4% greater proximity to the displacements of the intact mandible as compared to the hard design (Fig. 4b).

For craniocaudal (U_Z) displacement during LGF, the hard design performed better than the FGM[90–0] design. The hard design exhibited 25% less dissimilarity to the displacement patterns of the intact mandible, as compared to the FGM[90–0] design. The normalized cross-correlation between the intact mandible and the implanted mandible with a hard cartilage-mimicking component was −0.55, while it was −0.80 between the intact mandible and implanted mandible and the FGM[90–0] design (Fig. 4b). Additionally, the displacement pattern of the hard design was 3% closer to that of the intact mandible as compared to the FGM[90–0] design, as indicated by the corresponding Euclidean distances presented in Fig. 4b.

In the LGF scenario, the FGM[90–0] design showed better mediolateral (U_X) and anteroposterior (U_Y) displacements, while the hard cartilage design excelled in craniocaudal (U_Z) displacement. The displacement magnitudes showed that the FGM[90–0] design enhanced the mandibular movement range as compared to the hard design, with an average increase of 88%. The average displacement magnitude increased from 0.17 mm for the hard design to 0.32 mm for the FGM[90–0] design. Although the prosthesis with a hard cartilage-mimicking component exhibited 12% less dissimilarity from the displacement patterns observed in the intact mandible, as compared to the FGM[90–0] prosthesis (Fig. 4b), the FGM[90–0] design displayed a smaller average Euclidean distance (0.28 mm) to the intact mandible as compared to the hard design (0.34 mm). This indicates that the displacement of the FGM[90–0] design was 6% closer to the intact mandible (the average Euclidean distances in Fig. 4b). Consequently, with the FGM[90–0] design, there was an average performance increase of 19% during the INC and an average performance decrease of 3% during LGF. Additionally, the reaction forces on the prosthetic joint decreased from 151 N for the hard design to 137 N for the FGM[90–0] design, representing a reduction of nearly 10%.

The excessive mandibular displacements observed mediolaterally (U_X) and anteroposteriorly (U_Y) during biting, particularly during LGF, are due to the absence of the lateral pterygoid muscle, which controls the precise horizontal movement of the mandible[43]. Following TMJ replacement, translational movements are often the most impacted. The primary factors contributing to reduced mandibular translation include the detachment of the lateral pterygoid muscle, the geometry of the articular surface, and the development of fibrosis in the articular and muscular tissues[12].

Comparing the displacement patterns of implanted mandibles to that of the intact mandible during mastication is challenging, mainly due to their dependency on the prosthetic joint design approach[12,44,45]. The prosthetic joint is often simplified to be a spherical or ball-and-socket joint with a clearance between the articulating surfaces[2,12]. However, in this study, the prosthetic joint was designed with tight surface-to-surface contact. Since the TMJ is a bilateral joint, where the movement of one side affects the other, the implantation alters the kinematics of both the implanted and healthy sides of the mandible[9]. This interdependence complicates a direct comparison between the implanted and intact mandibles.

For a comparative analysis of various prosthesis designs, each implanted mandible can be positioned alongside an intact mandible[40]. The similarity (measured by α) and proximity (measured by the Euclidean distance) between the displacements of the intact and implanted mandibles largely depend on the design and modeling approach of the prosthetic joint. Ideally, α should be close to 1 and the Euclidean distance close to 0 when comparing the intact and implanted mandibles. However, it is important to recognize that α will not be exactly 1 and the Euclidean distance will not be exactly 0, as complete functional restoration of the TMJ is practically not achievable even with an effective replacement[46].

In this study, we designed artificial cartilage-mimicking components using FGMs, ranging from hard material properties to those of a softer material. In the actual TMJ prostheses, however, the implant is made of a cobalt-chromium-molybdenum alloy, a titanium alloy, or both, while the fossa component is typically made of polyethylene (UHMWPE)[47,48]. The resulting hard-soft contact interface without any gradual transitions poses risks of wear, slippage, and degradation over time[8,10,13]. Fabricating FGMs that transition from the metallic implant to the fossa component made of a soft material, such as polyethylene, is quite challenging.

To address this challenge, we suggest the use of multi-layer coatings on the metal implant to create functional gradation. Coatings can provide a softer region on the implant head, and reduce the risks associated with soft-hard contact while maintaining the structural integrity and durability of the metal implant. Additionally, introducing cellular structures made from the same material as the implant, with variations in porosity on the top of the implant using additive manufacturing techniques, such as directed energy deposition, could further enhance the gradation. This could be followed by the infiltration of a polymeric material to create FGMs.

Future research should focus on the development and testing of coating techniques and advanced manufacturing methods to enhance the performance and longevity of TMJ prostheses. Furthermore, performing fatigue tests on these designs will be crucial to evaluate their long-term durability and performance under physiological cyclic loading conditions. This will help in assessing the wear resistance and structural integrity of the prostheses over an extended period.

Methods

TMJ prosthesis design and manufacturing

The initial TMJ implant design was voxelized to fine voxel sizes of 0.25 × 0.25 × 0.25 mm^3 using a MATLAB code described in ref. 49 (Fig. 1b). Subsequently, ten (voxel) layers of materials, each with a thickness of 0.25 mm and an overall thickness of 2.5 mm (10 × 0.25 mm), were added onto the proximal part of the implant head to mimic the presence of the artificial cartilage (Fig. 1c). This design thickness falls within the average range measured for articular cartilage covering the temporomandibular joint disc, which varies between 2.0 and 2.8 mm in the central, lateral, medial, and posterior regions[50]. Each layer was then assigned a value of ρ, representing the volume fraction of the hard phase (Fig. 1c, d). In the original TMJ implant design, all voxels were consistently assigned a volume fraction of $\rho = 100\%$, indicating that they were entirely composed of the hard phase material. In the added ten layers positioned above the TMJ implant head, however, we assigned varied volume fractions of the hard phase, assigning values from $\rho = 90\%$ to $\rho = 0\%$ (Fig. 1c, d). This gradation in volume fraction created a functionally graded material, transitioning from the hard material of the implant to a softer material, thereby mimicking the function of natural cartilage.

We created five FGM artificial cartilages with varied material property distributions of $\rho = 0$, 10, 20, 30, 40, 50, 60, 70, 80, and 90% of the hard material, including (*i*) FGM[90–0] where the material distribution from the implant body toward the liner component was 90, 80, 70, 60, 50, 40, 30, 20,

Table 1 | FGM artificial cartilages with ten layers of varied material property distributions ρ(%) of the hard material

FGM design	material distribution ρ(%) within layers									
	L1	L2	L3	L4	L5	L6	L7	L8	L9	L10
FGM[90–0]	90	80	70	60	50	40	30	20	10	0
FGM [90–10]	90	80	70	60	50	40	30	20	10	10
FGM [90–20]	90	80	70	60	50	40	30	20	20	20
hard-soft	100	100	100	100	100	0	0	0	0	0
hard	100	100	100	100	100	100	100	100	100	100

The values are presented from left to right (L1–L10), indicating the distribution from the implant body toward the liner component.

10, and 0%, (*ii*) FGM [90–10] with a distribution of 90, 80, 70, 60, 50, 40, 30, 20, 10, and 10%, and (*iii*) FGM [90–20] with a distribution of 90, 80, 70, 60, 50, 40, 30, 20, 20, and 20%. We compared these designs with (*iv*) a cartilage-mimicking component having an abrupt hard-soft connection in the middle (denoted as 'hard-soft') with a distribution of 100, 100, 100, 100, 100, 0, 0, 0, 0, and 0%, and (*v*) a cartilage-mimicking component without a material gradient and with a volume fraction of $\rho = 100\%$ (denoted as 'hard') (Table 1 and Fig. 1d).

All the specimens were fabricated using a multi-material Polyjet 3D printer (ObjetJ735 Connex3, Stratasys® Ltd., USA) with a print resolution of 0.042 mm × 0.084 mm and a layer thickness of 0.027 mm[49]. Specimen preparation for printing was carried out using the GrabCAD Print software (Stratasys® Ltd., USA, version 1.76.10.25761). A rigid opaque photopolymer, VeroCyan™ (RGD841, Stratasys® Ltd., USA), was utilized to represent the hard phase, while a rubber-like photopolymer, Agilus30™ Clear (FLX935, Stratasys® Ltd., USA), was used for the soft phase. These materials, which are available in the 3D printer with different Shore hardness values, were automatically mixed by the 3D printer according to the specified volume fractions to achieve the desired material gradient.

Biomechanical testing

The healthy intact mandible and three prosthesis designs (*i.e.*, hard, hard-soft, and FGM[90–0]) were tested with three replications. To secure the connection of the TMJ implant to the mandible, we utilized universal flat head stainless-steel screws with dimensions of 3.0 × 12.0 mm. The torque applied during the screw insertion process was measured using a Stahlwille Torque Screwdriver 760 (Germany), with the maximum torque set at 0.3 Nm[51]. This ensured precise and controlled fixation of the implant.

The implanted and intact mandibles were biomechanically tested under quasi-static compressive loading using a mechanical testing bench (LLOYD instrument LR5K equipped with a 5000 N load cell) at a crosshead speed of 1 mm/min and with a preload of 10 N until failure occurred. The specimens were positioned upside down on the test setup proposed in ref. 52 (Fig. 1e). The load from the machine was distributed evenly in the region of the mandibular angle through a rigid steel bar. The cranial component with an (artificial) TMJ disk was used to support the condyle, constraining its translational movement while allowing rotational movement. The INC task was executed using a support structure that constrained the incisal region perpendicularly to the occlusion plane (*i.e.*, the *z*-direction) (Fig. 1e). Failure criteria included fractures of the mandible, the implant with the artificial cartilage, failure at the screw-substrate interface, or a crosshead displacement exceeding 10 mm after the preload.

The full-field strain and local deformation during the experimental testing were recorded using a Q-400 2 × 12 MPixel digital image correlation (DIC) system (LIMESS GmbH, Krefeld, Germany). Strain maps were generated at a frequency of 1 Hz with facet sizes ranging from 21 to 27 pixels. The lateral surface of the ramus bone and the TMJ implant together with the cartilage were designated as the region of interest (Fig. 2a). A black dot speckle pattern was applied over a white-painted background to cover the entire area of interest. Two digital cameras, along with LED panels for illumination, were positioned 0.7 m from the specimen to capture the images. Image processing and strain calculations were conducted using Istra4D x64 4.6.5 software (Dantec Dynamics A/S, Skovunde, Denmark). The maximum principal strain maps obtained from FEA were then compared to those measured with DIC within the linear region (Fig. 2a).

Computational modeling

The finite element analysis (FEA) was performed using the commercial software suite (implicit solver, Abaqus 2019, Dassault Systems Simulia, France). The model was developed based on the randomly selected and anonymized computed tomographic (CT) scan of a mandible described in[12] The CT data had a spatial resolution of 0.52×0.52×1.0 mm^3. The mandible segmentation was performed using Materialise Mimics® v21.0 (Materialise Inc., Leuven, Belgium), and Materialise 3-matic® v14.0 (Materialise Inc., Leuven, Belgium) was used for mesh generation. A quadratic tetrahedron (C3D10) element was used for both the implanted and intact mandibles. A model was accordingly created and accounted for nonlinear geometry to replicate the experimental condition (EXP-FEA) (see section 2.3.2 and Fig. 1e). Subsequently, the model was expanded to include a musculoskeletal system and simulate more complex physiological loading conditions (PHY-FEA), such as INC and LGF, according to the musculoskeletal model proposed by Korioth et al. [53] (Fig. 1f).

Material property assignments

The material properties of the hard phase (i.e., $\rho = 100\%$) were assigned to the implant body, while those of the FGM artificial cartilage were determined by the locally assigned volume fraction of the hard phase (ρ) to each individual layer. The constitutive model, which can predict both linear elastic and hyperelastic mechanical behaviors and accommodate both hardening or softening nonlinear regimes for a given volume fraction of the hard phase was obtained in our previous study[49]. However, here we only focused on the linear elastic part of these material properties.

In the EXP-FEA, all the components including the mandible, fossa component, cranial component, and TMJ disc were assumed to be isotropic and homogeneous and had linear elastic material properties ($E = 2697.3$ MPa and $\nu = 0.4$) for the hard phase (i.e., $\rho = 100\%$). In the PHY-FEA, the mandible was assumed to be isotropic and non-homogeneous, and have linear elastic material properties derived from the CT image data using Materialise Mimics® (Materialise Inc., Leuven, Belgium) as described in ref. 12. The material properties of the TMJ disc and cranial component were set to be homogeneous, isotropic, and linearly elastic, as described in ref. 12,40.

Loads and boundary conditions

The model was constrained at the superior surfaces of both cranial sections in all directions (Fig. 1e, f). Biting tasks were simulated by constraining the teeth in the direction perpendicular to the plane of occlusion (*i.e.*, the *z*-direction) (Fig. 1e, f). In other words, no vertical movements of the lateral and central incisors were allowed during INC.

The interactions between the cartilage (i.e., TMJ disc) and cranial component and between the fossa component and cranial component were modeled with a tie constraint. The contacts between the cartilage

Table 2 | Muscle force components (25% of maximum bite force) for the incisal clenching (INC) and left group (LGF) biting tasks

Muscle name	Incisal clenching (INC)			Left group biting (LGF)		
	F_x [N]	F_y [N]	F_z [N]	F_x [N]	F_y [N]	F_z [N]
Right masseter	−30.46	−27.09	92.89	−24.80	−15.57	68.66
Left masseter	30.46	−27.09	92.89	25.81	−4.30	58.65
Right temporalis	−4.22	5.46	20.85	−4.31	6.99	19.95
Left temporalis	4.22	5.46	20.85	43.38	73.77	196.93
Right lateral pterygoid	45.48	−50.35	−8.02	8.53	−9.56	−1.63
Left lateral pterygoid	−45.48	−50.35	−8.02	−32.62	−37.47	−7.19
Right medial pterygoid	73.76	−56.61	120.06	72.02	−55.27	117.21
Left medial pterygoid	−73.76	−56.61	120.06	−6.63	−5.09	10.80
Right anterior digastric	−5.44	20.95	−5.28	−4.14	15.95	−4.02
Left anterior digastric	5.44	20.95	−5.28	5.56	21.41	−5.40

(TMJ disc) and mandibular condyle and between the mandible and the TMJ implant were assumed to be frictionless. Fixation screws were modeled by applying a rigid beam constraint to the adjacent screw hole surfaces of the TMJ implant and the bone. A bar-to-bone contact was modeled using a friction coefficient (penalty) of 0.2 and a finite sliding formulation without surface smoothing[52].

In EXP-FEA, a steel loading bar was simulated as an analytically rigid and, thus, non-deformable object. The bar was placed to transmit distributed forces similar to those applied in the experiments (Fig. 1e). A displacement of 2 mm was imposed on the bar along the positive z-direction (craniocaudal axis) with all the rotations constrained except for those around the y-axis (anteroposterior axis).

In PHY-FEA, the FGM-incorporated prostheses were subjected to conditions under INC and LGF biting tasks. Table 2 lists the muscle force components for each biting task. To ensure that the TMJ prosthesis experiences a maximum stress level below the yield stress of the soft material, we considered 25% of the maximum muscle forces for INC and LGF from the literature[12,40]. Moreover, the left lateral pterygoid muscle was detached in the implanted model. Each muscle force was applied as a concentrated load at the corresponding insertion point (Fig. 1f). Nodes within a 2 mm radius of each insertion point were kinematically coupled to the corresponding node to simulate realistic muscle forces. These boundary conditions were selected based on their widespread use and recognition in the literature for accurately simulating TMJ function under physiological loading conditions[9,12,40,52,53].

Kinematic performance evaluation

We assessed the functional performance of the designs by analyzing mandibular displacement during INC and LGF biting tasks, and compared mediolateral, anteroposterior, and craniocaudal displacements (Figs. 3 and 4). Moreover, we evaluated the joint reaction forces for each design by measuring the forces exerted at the artificial joint interfaces during these tasks using the finite element model.

To do this, we selected a series of sampling points along the lower contour of the mandible. For a symmetrical configuration, points on one half of the mandible were chosen at nearly equal distances, and these points were then mirrored across the sagittal plane to ensure symmetry (Fig. 3a). We calculated the displacements at each sampling point using the finite element model. We then compared the displacement of each sampling point between the intact and implanted mandibles using normalized cross-correlation, represented by Pearson's correlation coefficient (α),

$$\alpha = \frac{\sum_i^n \left(U_i^{intact} - \bar{U}^{intact}\right)\left(U_i^{implanted} - \bar{U}^{implanted}\right)}{\sqrt{\sum_i^n \left(U_i^{intact} - \bar{U}^{intact}\right)^2 \sum_i^n \left(U_i^{implanted} - \bar{U}^{implanted}\right)^2}} \quad (1)$$

where U_i^{intact} represents the displacement of i^{th} sampling point out of n sampling points on the intact mandible, $U_i^{implanted}$ represents the displacement of i^{th} sampling point on the implanted mandible, $\bar{U}^{intact}$ is the mean displacement of all the sampling points on the intact mandible, and $\bar{U}^{implanted}$ is the mean displacement of all the sampling points on the implanted mandible.

Furthermore, to quantify the spatial differences between the corresponding displacement sampling points of the intact and implanted mandibles, the Euclidean distance was calculated (Fig. 4b):

$$Euclidean\ distance = \sqrt{\sum_i \left(U_i^{intact} - U_i^{implanted}\right)^2} \quad (2)$$

Conclusions

This study investigated the incorporation of FGMs into TMJ prostheses to enhance mandibular kinematics and reduce prosthesis reaction forces. We tested various FGM configurations with different material property distributions and compared them with the designs featuring an abrupt soft-hard transition and no gradient. An experimentally validated finite element model was used to evaluate the designs under INC and LGF tasks. The results demonstrate that the prosthesis with an abrupt hard-soft connection in the cartilage suffers from stress concentrations; the stress at the interface is increased by up to nine times as high as that of the FGM[90–0] cartilage design. The FGM[90–0] cartilage design improves the performance by 19% during the INC and decreases performance by 3% during LGF in terms of mandibular kinematics and reduces the joint reaction force by 8% and 10% at the artificial joint interfaces during the INC and LGF, respectively. Additionally, the FGM[90–0] design makes the mandibular movement less asymmetric during the INC. The FGM[90–0] cartilage design significantly increases the mandibular movement range by 20% during the INC and 88% during LGF as compared to the hard design. Although FGM-incorporated prostheses show great promise in enhancing TMJ functionality, achieving a complete replication of the natural TMJ function remains challenging and the fabrication technology for such protheses are yet to be developed.

Data availability

The data that support the findings of this study will be provided upon reasonable request.

Received: 18 July 2024; Accepted: 30 September 2024;
Published online: 12 October 2024

References

1. Guarda-Nardini, L., Manfredini, D. & Ferronato, G. Temporomandibular joint total replacement prosthesis: current knowledge and considerations for the future. *Int. J. Oral. Maxillofac. Surg.* **37**, 103–110 (2008).
2. Sinno, H., Tahiri, Y., Gilardino, M. & Bobyn, D. Engineering alloplastic temporomandibular joint replacements. *McGill J. Med.* **13**, 63 (2011).
3. Wilkie, G. & Al-Ani, Z. Temporomandibular joint anatomy, function and clinical relevance. *Br. Dent. J.* **233**, 539–546 (2022).
4. Minervini, G. et al. Pharmacological therapy in the management of temporomandibular disorders and orofacial pain: a systematic review and meta-analysis. *BMC Oral. Health* **24**, 78 (2024).
5. Yap, A. U., Lei, J., Liu, C. & Fu, K.-Y. Comparison of painful temporomandibular disorders, psychological characteristics, sleep quality, and oral health-related quality of life of patients seeking care

before and during the Covid-19 pandemic. *BMC Oral. Health* **23**, 438 (2023).
6. Ilgunas, A. et al. Patients' experiences of temporomandibular disorders and related treatment. *BMC Oral. Health* **23**, 653 (2023).
7. Westermark, A., Koppel, D. & Leiggener, C. Condylar replacement alone is not sufficient for prosthetic reconstruction of the temporomandibular joint. *Int. J. Oral. Maxillofac. Surg.* **35**, 488–492 (2006).
8. Gonzalez-Perez-Somarriba, B., Centeno, G., Vallellano, C. & Gonzalez-Perez, L. M. On the Analysis of the Contact Conditions in Temporomandibular Joint Prostheses. *Adv. Mater. Sci. Eng.* **2018**, 2687864 (2018).
9. van Loon, J.-P., Otten, E., Falkenström, C. H., de Bont, L. G. M. & Verkerke, G. J. Loading of a unilateral temporomandibular joint prosthesis: A three-dimensional mathematical study. *J. Dent. Res.* **77**, 1939–1947 (1998).
10. Dolwick, M. Reconstruction of the TMJ using an alloplastic stock total joint prostheses. *Int. J. Oral. Maxillofac. Surg.* **40**, 1015 (2011).
11. Mercuri, L. G. *Temporomandibular Joint Total Joint Replacement—TMJ TJR* (Springer Int Pub, 2016).
12. Pinheiro, M., Willaert, R., Khan, A., Krairi, A. & Van Paepegem, W. Biomechanical evaluation of the human mandible after temporomandibular joint replacement under different biting conditions. *Sci. Rep.* **11**, 14034 (2021).
13. Pinto-Borges, H. et al. A preliminary analysis of the wear pathways of sliding contacts on temporomandibular joint total joint replacement prostheses. *Metals* **11**, 685 (2021).
14. Leiggener, C., Erni, S. & Gallo, L. Novel approach to the study of jaw kinematics in an alloplastic TMJ reconstruction. *Int. J. Oral. Maxillofac. Surg.* **41**, 1041–1045 (2012).
15. Van Loon, J.-P., Falkenström, C., De Bont, L., Verkerke, G. & Stegenga, B. The theoretical optimal center of rotation for a temporomandibular joint prosthesis: a three-dimensional kinematic study. *J. Dent. Res.* **78**, 43–48 (1999).
16. Perez, D., Perez, L., Mahgoub, H. & Hernandez, N. Subjective and functional outcomes following TMJ reconstruction with custom-made total joint prostheses. *J. Oral. Maxillofac. Surg.* **72**, e15 (2014).
17. Quan, S., Kaide, L. & Lei, L. Progress of temporomandibular joint prosthesis. *West China J. Stomatol.* **32**, 422–425 (2014).
18. van Kootwijk, A. et al. Biomechanical evaluation of additively manufactured patient-specific mandibular cage implants designed with a semi-automated workflow: A cadaveric and retrospective case study. *J. Mech. Behav. Biomed. Mater.* **146**, 106097 (2023).
19. Brouwer de Koning, S. G. et al. Design considerations for patient-specific bone fixation plates: A literature review. *Med. Biol. Eng. Comput.* **61**, 3233-3252 (2023).
20. Idogava, H. T., Noritomi, P. Y. & Daniel, G. B. Numerical model proposed for a temporomandibular joint prosthesis based on the recovery of the healthy movement. *Comput. Methods Biomech. Biomed. Eng.* **21**, 503–511 (2018).
21. Mirzaali, M. J., Moosabeiki, V., Rajaai, S. M., Zhou, J. & Zadpoor, A. A. Additive manufacturing of biomaterials—Design principles and their implementation. *Materials* **15**, 5457 (2022).
22. Saldívar, M. C. et al. Rational positioning of 3D-printed voxels to realize high-fidelity multifunctional soft-hard interfaces. *Cell Rep. Phys. Sci.* **4** (2023).
23. Mirzaali, M. J. et al. Mechanics of bioinspired functionally graded soft-hard composites made by multi-material 3D printing. *Compos. Struct.* **237**, 111867 (2020).
24. Mirzaali, M. J. et al. Multi-material 3D printing of functionally graded hierarchical soft–hard composites. *Adv. Eng. Mater.* **22**, 1901142 (2020).
25. Liu, Y. X., Thomopoulos, S., Birman, V., Li, J. S. & Genin, G. M. Bi-material attachment through a compliant interfacial system at the tendon-to-bone insertion site. *Mech. Mater.* **44**, 83–92 (2012).
26. Genin, G. M. et al. Functional grading of mineral and collagen in the attachment of tendon to bone. *Biophys. J.* **97**, 976–985 (2009).
27. Sola, A., Bellucci, D. & Cannillo, V. Functionally graded materials for orthopedic applications–an update on design and manufacturing. *Biotechnol. Adv.* **34**, 504–531 (2016).
28. Saldívar, M. C. et al. Bioinspired rational design of bi-material 3D printed soft-hard interfaces. *Nat. Commun.* **14**, 7919 (2023).
29. Ren, L. et al. Graded biological materials and additive manufacturing technologies for producing bioinspired graded materials: An overview. *Compos. B: Eng.* **242**, 110086 (2022).
30. Pandey, P. M., Rathee, S., Srivastava, M. & Jain, P. K. *Functionally Graded Materials (FGMs): Fabrication, properties, Applications, and Advancements* (CRC Press, 2021).
31. Knoppers, G., Gunnink, J., Van Den Hout, J. & Van Vliet, W. The reality of functionally graded material products. In: *Proc. 2004 International Solid Freeform Fabrication Symposium, Austin, TX* 38–43 (2004).
32. Bohidar, S. K., Sharma, R. & Mishra, P. R. Functionally graded materials: a critical review. *Int. J. Res.* **1**, 289–301 (2014).
33. Naebe, M. & Shirvanimoghaddam, K. Functionally graded materials: a review of fabrication and properties. *Appl. Mater. Today* **5**, 223–245 (2016).
34. Elleuch, S., Jrad, H., Wali, M. & Dammak, F. Mandibular bone remodeling around osseointegrated functionally graded biomaterial implant using three dimensional finite element model. *Int. J. Numer. Methods Biomed. Eng.* **39**, e3750 (2023).
35. Ayatollahi, M. R., Davari, M. H., Shirazi, H. A. & Asnafi, A. To improve total knee prostheses performance using three-phase ceramic-based functionally graded biomaterials. *Front. Mater.* **6** (2019).
36. Jyoti & Ghosh, R. Printable functionally graded tibial implant for TAR: FE study comparing implant materials, FGM properties, and implant designs. *Comput. Biol. Med.* **177**, 108645 (2024).
37. Hedia, H. S., Aldousari, S. M., Abdellatif, A. K. & Fouda, N. A new design of cemented stem using functionally graded materials (FGM). *Bio-Med. Mater. Eng.* **24**, 1575–1588 (2014).
38. Najibi, A. & Mokhtari, T. Functionally graded materials for knee and hip arthroplasty; an update on design, optimization, and manufacturing. *Compos. Struct.* **322**, 117350 (2023).
39. Mehrali, M. et al. Dental implants from functionally graded materials. *J. Biomed. Mater. Res. A* **101**, 3046–3057 (2013).
40. Pinheiro, M., Krairi, A., Willaert, R., Costa, M. C. & Van Paepegem, W. Structural optimization of patient-specific temporomandibular joint replacement implants for additive manufacturing: novel metrics for safety evaluation and biomechanical performance. *Bio-Des. Manuf.* **5**, 333–347 (2022).
41. Szykiedans, K. & Credo, W. Mechanical properties of FDM and SLA low-cost 3-D prints. *Procedia Eng.* **136**, 257–262 (2016).
42. Lin, D., Li, Q., Li, W. & Swain, M. Dental implant induced bone remodeling and associated algorithms. *J. Mech. Behav. Biomed. Mater.* **2**, 410–432 (2009).
43. Murray, G. M., Phanachet, I., Uchida, S. & Whittle, T. The role of the human lateral pterygoid muscle in the control of horizontal jaw movements. *J. Oral. Facial Pain. Headache* **15**, 279–92 (2001).
44. Madhavan, S., Dhanraj, M. & Jain, A. R. Methods of recording mandibular movements—a review. *Drug Invent. Today* **10**, 1254–1259 (2018).
45. Xu, X., Luo, D., Guo, C. & Rong, Q. A custom-made temporomandibular joint prosthesis for fabrication by selective laser melting: Finite element analysis. *Med Eng. Phys.* **46**, 1–11 (2017).
46. Oldhoff, M., Mirzaali, M. J., Tümer, N., Zhou, J. & Zadpoor, A. Comparison in clinical performance of surgical guides for mandibular surgery and temporomandibular joint implants fabricated by additive manufacturing techniques. *J. Mech. Behav. Biomed. Mater.* **119**, 104512 (2021).
47. De Meurechy, N., Braem, A. & Mommaerts, M. Y. Biomaterials in temporomandibular joint replacement: current status and future

perspectives—a narrative review. *Int. J. Oral. Maxillofac. Surg.* **47**, 518–533 (2018).
48. McCoy, R. J. & Psutka, D. J. *Alloplastic Temporomandibular Total Joint Replacement, Diagnosing and Managing Temporomandibular Joint Conditions* (ed. Machon, V.) (IntechOpen, 2024).
49. Saldívar, M. C., Doubrovski, E. L., Mirzaali, M. J. & Zadpoor, A. A. Nonlinear coarse-graining models for 3D printed multi-material biomimetic composites. *Addit. Manuf.* **58**, 103062 (2022).
50. Mirahmadi, F., Koolstra, J. H., Lobbezoo, F., van Lenthe, G. H. & Everts, V. Ex vivo thickness measurement of cartilage covering the temporomandibular joint. *J. Biomech.* **52**, 165–168 (2017).
51. Ramos, A., Duarte, R. J. & Mesnard, M. Strain induced in the condyle by self-tapping screws in the Biomet alloplastic temporomandibular joint: a preliminary experimental study. *Int. J. Oral. Maxillofac. Surg.* **44**, 1376–1382 (2015).
52. van Kootwijk, A. et al. Semi-automated digital workflow to design and evaluate patient-specific mandibular reconstruction implants. *J. Mech. Behav. Biomed. Mater.* **132**, 105291 (2022).
53. Korioth, T. W. P. & Hannam, A. G. Deformation of the human mandible during simulated tooth clenching. *J. Dent. Res.* **73**, 56–66 (1994).

Acknowledgements

M.J.M. acknowledges funding from the Open Competition Domain Science – XS, NWO, and the Idea Generator (NWA-IDG) research program, under grant numbers NWA.1228.192.228. J.Z. and A.A.Z. acknowledge funding from the 3DMED project, which has received support from the Interreg 2 Seas program 2014–2020, co-funded by the European Regional Development Fund under subsidy contract No. 2S04-014.

Author contributions

V.M.: Conceptualization, Investigation, Formal analysis, Methodology, Visualization, Writing—Original Draft. A.K.: Conceptualization, Investigation, Formal Analysis, Methodology, Visualization, Writing–Review & Editing. M.C.S.: Investigation. W.V.P.: Conceptualization, Investigation, Writing–Review & Editing. B.P.J.: Writing–Review & Editing. E.B.W.: Writing—Review & Editing. J.Z.: Conceptualization, Investigation, Formal Analysis, Writing—Review & Editing. N.T.: Conceptualization, Investigation, Formal analysis, Methodology, Supervision, Writing—Review & Editing. M.J.M.: Conceptualization, Investigation, Formal analysis, Methodology, Supervision, Funding Acquisition, Resources, Writing–Review & Editing. A.A.Z.: Investigation, Supervision, Funding Acquisition, Resources, Writing—Review & Editing. All authors have read and agreed to the published version of the manuscript.

Competing interests

The authors declare no competing interests.

Additional information

Supplementary information The online version contains supplementary material available at https://doi.org/10.1038/s43246-024-00664-4.

Correspondence and requests for materials should be addressed to Vahid Moosabeiki or Mohammad J. Mirzaali.

Peer review information *Communications materials* thanks Amir Najibi and the other, anonymous, reviewer(s) for their contribution to the peer review of this work. Primary Handling Editors: Jet-Sing Lee. A peer review file is available.